Construction Co-ZnO acid-base pair catalysts for alcohol and nitrobenzene hydrogen transfer cascade reaction

Zhanwei Chen [a,1], Chen Wu [a,1], Wenrui Li [a], Shaowei Yang [a], Haidong Shen [a], Runze Gao [a], Tianshuai Wang [a,b,*], Qiuyu Zhang [a], Hepeng Zhang [a,**]

[a] Xi'an Key Laboratory of Functional Organic Porous Materials, School of Chemistry and Chemical Engineering, Northwestern Polytechnical University, Xi'an 710129, PR China
[b] Chongqing Science and Technology Innovation Center of Northwestern Polytechnical University, Chongqing 401135, PR China

ARTICLE INFO

ABSTRACT

The strength and micro-distance of acidic and basic sites on acid-base pair catalysts (ABPC) are crucial in determining their synergistic effect and catalytic capacity, yet challenging in the synthesis of effective ABPC due to the tunable difficulties. Here, a Co-ZnO ABPC, containing adjacent Co single atoms-ZnO nanocluster acid-base pairs, was prepared by pyrolyzing ZnCo ZIF-precursor under vacuum. Benefiting from the unique acid-base pair features, Co-ZnO ABPC exhibited outstanding performance for the catalytic hydrogen transfer (CHT) cascade reaction, achieving high nitrobenzene conversion (95 %) and imine selectivity (98 %) at 160 °C for 3 h, exceeded almost all the documented catalysts. Both the experimental and calculation results verified the stronger acidity of Co SAs and the synergistic effect of acid-base sites lowered the free energy barrier. This work provides not only prospective insight into the effect of acid-base sites on the catalytic capacity but also a guide for the rational design of efficient ABPC.

1. Introduction

As one of the most important materials, acid-base site pair catalysts (denoted as ABPC) can be used in a wide range of reactions, including the oxidation of alcohols to enhance the reaction rate and lower the reactive conditions, therefore attracting intense investigations to persistently improve their catalytic performance [1–4]. The strength and micro-distance of acidic and basic sites are crucial in determining their synergistic effect and catalytic capacity. For example, during the oxidation process (Scheme 1a), the O atom of hydroxymethyl can be attracted by the acidic site, while the H of –OH or –CH₂ can be removed with the assistance of the adjacent basic site [5]. In this situation, the strength of the acidic site will affect its interaction with the O atom, thereby influencing the degree to which the O–H or C–H bonds are weakened. Moreover, the strength and location of the basic site will importantly affect the dehydrogenation, so it must be situated near the H atom of O–H or C–H. However, engineering of acidic and basic sites,

especially structuring suitable basic sites near the acidic sites, is a challenging task owing to its micro-characteristic. Therefore, to complement the insufficient basic sites of ABPC, bases, such as NaOH or Na₂CO₃ et al., were added to improve the catalytic performance [6,7]. Nevertheless, the additional consumption of base not only increases the cost but also causes environmental issues. Consequently, designing and preparing efficient ABPC has become highly desirable.

Imines are compounds containing C=N double bonds and are of great importance in the fields of medicine, biology, functional materials, and catalysis [8–13]. Traditionally, imines are prepared by condensation of aldehydes and amines, nitrile hydrogenation, self-coupling of primary amines, or coupling of alcohols and amines [14–19]. However, these methods suffer from valuableness, inferior stability of reactants, the need for excessive exogenous bases and hydrogen donors [20]. Therefore, the direct reductive coupling of nitro compounds with alcohols to synthesize imines through catalytic hydrogen transfer (CHT) cascade reactions (Scheme 1b) has attracted considerable interest due to

---

its atomic economy and green process. In the past, catalysts based on noble metals such as Pd [21], Ru [22], Au [23] and Rh [24] have been demonstrated to be effective in CHT cascade reactions. However, the expensive and scarce characteristics impede their practical applications. Our groups have developed one nano-pyramid-type Co-ZnO/NC catalyst [5], and benefiting its unique structure and acid-base site, Co-ZnO/NC achieved a high nitrobenzene conversion, imine selectivity, and turnover frequency under an ambient inert atmosphere at 160 °C for 4 h with a theoretical molar ratio of nitrobenzene to benzyl alcohol (1/3). Nevertheless, to meet the demands of practical applications, catalysts with higher efficiency must be structured to more gentle reaction conditions.

Based on the characteristic of the CHT cascade reactions, it is challenging to achieve satisfactory reaction activity using catalysts with a single active site. Therefore, rationally designing the type and microconstructure of acidic and basic sites in ABPC is an effective approach to address the issues mentioned above. According to our previous research, Co single atoms (SAs) are efficient acidic sites for the adsorption and activation of hydroxymethyl, while the relatively weak basic strength of N, coordination atoms with Co SAs, hampers the catalytic activity of Co SAs catalysts [25,26]. ZnO, an amphoteric oxide, is suitable for catalyzing the CHT cascade reaction as a basic site due to its invariable valence state and immobile lattice oxygen [27–29]. However, preparing catalyst with Co SAs located close to ZnO remains a significant challenge.

Herein, a novel Co-ZnO acid-base pairs catalyst (denoted as Co-ZnO ABPC) was prepared by controlled pyrolysis of ZnCo ZIF-precursor at 800 °C under vacuum. Benefiting from the vacuum effect during pyrolysis, Co-ZnO ABPC possessed substantial adjacent Co-ZnO or Zn-ZnO acid-base pairs on the surface of nitrogen doped-carbon (donated as CN). The unique acid-base pair structure design for the coexistence of Co SAs as the acidic sites and ZnO nanoclusters as the basic sites endowed Co-ZnO ABPC outstanding catalytic performance for the CHT cascade reaction, the conversion of nitrobenzene and the selectivity of imine reached 95 % and 98 %, respectively, under a N$_2$ atmosphere at 160 ℃ for 3 h with a nitrobenzene to benzyl alcohol molar ratio of 1/3. Moreover, the two above values of 97 % and 99 % were even achieved ever at 120 ℃ for 12 h in the presence of K$_2$CO$_3$, which exceeded almost all the documented catalysts (Table S1 and Table 1 entry 8). In addition, Co-ZnO ABPC possessed excellent durability and universality. First principle calculations and experimental comparisons revealed that Co-ZnO acid-base pairs were the primary reactive sites, and moreover, the reaction mechanism also was inferred.

2. Experimental

2.1. Materials and reagents

Dimethyl imidazole (MeIM) was purchased from Aladdin Reagent Co., Ltd (Shanghai, China). Zinc nitrate hexahydrate (Zn(NO$_3$)$_2$·6 H$_2$O), cobalt nitrate hexahydrate (Co(NO$_3$)$_2$·6H$_2$O), nitrobenzene, benzyl alcohol, toluene, methanol, and ethanol were obtained from Guangdong Guanghua Technology Co., Ltd. Dodecane was purchased from Sigma Company. The above reagents were of analytical grade and used directly without any further purification before the experiment. Deionized water used in the experiments was from local sources.

2.2. Catalysts preparation

2.2.1. Preparation of Zn-ZIF and ZnCo-ZIF precursors

During the typical synthesis procedure, a 7.5 mmol mixture of Co (NO$_3$)$_2$·6H$_2$O and Zn (NO$_3$)$_2$·6H$_2$O was dispersed in 75 ml methanol. This mixture was then quickly poured into a solution of 15.0 mmol MeIM in methanol. After ultrasonic mixing for 5 min, the resulting slurry was maintained at room temperature for 4 h. These obtained solids were washed several times with methanol through centrifugation and subsequently dried under vacuum at 60 °C overnight. The products obtained were labeled as Zn-ZIF (no cobalt addition) and ZnCo-ZIF (with a Zn/Co ratio of 1:1), respectively.

2.2.2. Preparation of Co-ZnO ABPC and Zn-ZnO ABPC

The as-synthesized ZIFs precursors were placed in a tubular furnace, in which the pressure remained at ΔP= −0.05 MPa after repeatedly washing by nitrogen gas. The sample was heated to 800 °C and kept for 3 h within the pressure with a heating rate of 5 °C/min.

2.2.3. Preparation of ZnCo -N$_2$/CN

The as-synthesized ZnCo-ZIF was placed in a tubular furnace and heated from room temperature to 800 °C at a heating rate of 5 °C/min and kept for 3 h under N$_2$ flow.

2.2.4. Preparation of Co-ZnO ABPC-H, Zn-ZnO ABPC-H and ZnCo- N$_2$/CN -H

The as-synthesized catalysts were etched in 3 M HCl solution for 24 h at 80 °C. Finally, the resulting products were filtrated and washed with deionized water several times until the filtrate was neutral and dried at 60 °C in the oven.
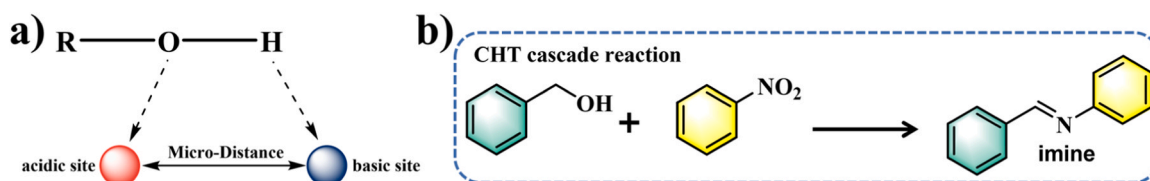
2.3. Catalysts evaluation

In a typical CHT cascade reaction involving benzyl alcohol (A) and nitrobenzene (B), the catalyst (20 mg) was added to a mixture consisting of 1.0 mmol nitrobenzene and 3.0 mmol benzyl alcohol, which was dissolved in 1.0 ml toluene as the solvent. The mixture was then placed in a Teflon-lined stainless autoclave reactor with a capacity of 50 ml. The sealed reactor was purged with N$_2$ three times, and subsequently heated to 160 °C and kept for 3 h.

After the reaction, the mixture was diluted with ethanol and centrifuged. The conversion of the reactant (nitrobenzene) and the yield of the imine product (N-benzylidene aniline, C) were measured by a gas chromatograph (GC, FULI GC 9720 plus) with SE-54 capillary column (30 m × 0.32 mm ×0.5 µm) equipped with a flame ionization detector (FID) using dodecane as the internal standard. The operating conditions were as follows: the flow rate of the N$_2$ carrier gas was 30 ml/min; the injection port temperature was 250 °C. The GC oven temperature program was as follows: first held at 100 °C for 1 min, then increased from 100 °C to 180 °C with a heating rate of 10 °C/min, then increasing from 180 °C to 250 °C with a heating rate of 20 °C/min, finally holding at 250 °C for 2 min
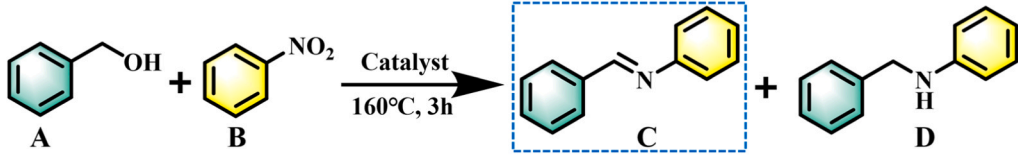
The nitrobenzene conversion (Con_B) is defined by:

$$Con_B(\%) = \frac{n_B - n_B^{'}}{n_B} \times 100$$

Scheme 1. (a) The synergistic effect of acid-base sites for alcohol oxidation and (b) Imine synthetic method by CHT cascade reaction.

Table 1
CHT cascade reaction results between nitrobenzene and benzyl alcohol catalyzed by the obtained materials.

Aimed Product

Entry	Catalyst	Base	$Con_B\%$	$Sel_C\%$	$Sel_D\%$
1	Co-ZnO ABPC	None	95	98	2
2[a]	Co-ZnO ABPC-H	None	-	-	-
3[a]	Zn-ZnO ABPC-H	None	-	-	-
4[a]	Co SAC/CN[b]	None	-	-	-
5[a]	ZnO/AC[c]	None	-	-	-
6[a]	Zn-ZnO ABPC	None	17	100	-
7[a]	Co-ZnO ABPC	None	61	98	2
8[a]	Co-ZnO ABPC	K_2CO_3[d]	97	99	1
9[a]	Co-ZnO ABPC-H	K_2CO_3[d]	76	99	1
10[a]	Zn-ZnO ABPC-H	K_2CO_3[d]	14	100	-
11[a]	Co SAC/CN[b]	K_2CO_3[d]	75	99	1
12[a]	None	K_2CO_3[d]	-	-	-

Reaction conditions: 3 mmol benzyl alcohol, 1 mmol nitrobenzene, 20 mg catalyst, 1 ml toluene, 160 ℃, 3 h, N_2. The conversion and yield were determined by GC. [a] At 120 ℃, 12 h; [b] Vacuum calcination of ZnCo-ZIF at 1000 °C followed by etching to obtain Co SAC/CN; [c] ZnO/AC was obtained by impregnation method and calcinating the precursor under an inert atmosphere at 900 °C for 3 h; [d] 10 % mol K_2CO_3 is added.

and the yield of imine (Yie_C) is calculated based on nitrobenzene conversion by:

$$Yie_C(\%) = \frac{n_C^{'}}{n_B} \times 100$$

Hence, the selectivity of imine (Sel_C) based on nitrobenzene conversion can be expressed as:

$$Sel_C(\%) = \frac{Yie_C}{Con_B} \times 100$$

Where:

n_B: the molar amount of nitrobenzene added in the reaction system, mmol;

$n_B^{'}$: the molar amount of nitrobenzene in the reaction system after the reaction, mmol;

$n_C^{'}$: the molar amount of imine in the reaction system after the reaction, mmol.

Turnover frequency (TOF, $mmol_{converted\ nitrobenzene}\ mmol_{total}^{-1}\ h^{-1}$) could be expressed as:

$$TOF = \frac{n_B * Con_B\%}{\left(\frac{Zn\ wt\%}{M_{Zn}} + \frac{Co\ wt\%}{M_{Co}}\right) * m * t}$$

Where:

n_B: the molar amount of nitrobenzene added in the reaction system, mmol;

Con_B: the nitrobenzene conversion was determined by GC using dodecane as an internal, %;

Co wt% and *Zn wt%*: the cobalt and zinc contents in the catalysts which are determined by ICP-MS;

M_{Co}: the molar mass of Co, 58.93 g/mol;

M_{Zn}: the molar mass of Zn, 65.41 g/mol;

m: the mass amount of the metal species measured by ICP-MS, g;

t: reaction time, h.

2.4. Characterization

Powder X-ray diffraction patterns of both ZIF and carbon materials were recorded on a Bruker D8 DISCOVER A25 X-ray diffractometer (Germany) with Co Kα radiation (3 kV). The samples' morphology and structure were studied using field-emission scanning electron microscope (FE-SEM, FEI Verious G4) and transmission electron microscopy (TEM, FEI Talos F200X TEM operated at 200 kV). Co and Zn contents were obtained on Inductively Coupled Plasma Mass Spectrometer (ICP-MS, NexION™ 350D PerkinElmer USA). X-ray diffraction patterns (XRD) were recorded using X-ray powder diffraction (XRD-7000S from Shimadzu) to characterize the structure and crystallinity of the samples. N_2-adsorption desorption isotherms and pore size distributions were obtained using the 3 H-2000PS2 type PS2–0790 Surface Area Porosity Analyzer from Beishide Instrument Technology (Beijing) Co., Ltd. The samples were degassed at 80 oC for 4 h under vacuum before testing. The specific surface area and pore volume were calculated from the Brunauer-Emmett-Teller (BET) and Barrett-Joyner-Halenda (BJH) methods, respectively. X-ray photoelectron spectroscopy (XPS) measurements were performed with an Axis Ultra DLD X-ray photoelectron spectroscopy manufactured by Kratos Company in the United Kingdom. The instrument used an Al K α ray light source to measure the total ambient gas pressure ($<10^{-8}$ Pa). NH_3 temperature-programmed desorption (NH_3-TPD) and CO_2 temperature-programmed desorption (CO_2-TPD) were carried out on a Micromeritics Autochem II chemisorption analyzer. 50 mg sample loaded in a quartz reactor was pretreated with Ar at 500 ℃. After cooling to 50 ℃, NH_3 or CO_2 adsorption was performed by switching Ar to NH_3 or CO_2 gas and then maintaining 2 h. After adsorption, the physical adsorption of NH_3 or CO_2 was removed at the same temperature by Ar purging for 1 h. Then, TPD was detected by Thermal Conductive Detector (TCD) in the Ar flow by raising the temperature to 700 ℃ at a rate of 10 ℃/min.

2.5. Computational methods

The projector augmented wave (PAW) formalism of density functional theory as implemented in the Vienna Ab-initio Simulation Package (VASP) was used in the system energy and electronic structure calculations [30]. The Gaussian smearing method was used, and the width of smearing was chosen as 0.05 eV. The energy cutoff for plane-wave expansion of the PAWs is 500 eV. The optimized lattice constants of bulk ZnO are a= 3.24 Å and c= 5.19 Å, and the lattice constants of graphene are 2.48 Å. Both are in good agreement with the experimentally measured values. A four atomic layer of ZnO (100) slab with a 3 × 2 supercell was constructed for the ZnO surface system. In the

vertical direction, a vacuum layer of about 15 Å in thickness was introduced for all the surfaces. For the adsorption energy simulations, we used the DFT-D3 functional to include the physical van der Waals interaction [31]. The adsorption energy (E_{ad}) of adsorbate is defined as $E_{ad} = E_T - E_0 - E_B$, where E_0 is the energy of the surface investigated, E_T is the energy of the corresponding system with adsorbate, E_B is the energy of adsorbate molecule, respectively. The larger the negative value of E_{ad}, the stronger the interaction between the adsorption systems. The Brillouin zone was sampled using the Monkhorst-Pack scheme with a k-point mesh of $3 \times 3 \times 1$ in the Gamma-centered grids for the

structural relaxation [32]. The structure relaxation was continued until the forces on all the atoms were converged to less than 0.01 eV/Å.

3. Results and discussion

3.1. Catalyst synthesis and characterizations

The designed Co-ZnO ABPC was prepared by a two steps method (Fig. 1a): (1) synthesis of ZnCo-ZIF precursor with a suitable Zn/Co ratio and (2) controlled pyrolysis of the ZnCo-ZIF precursor under vacuum
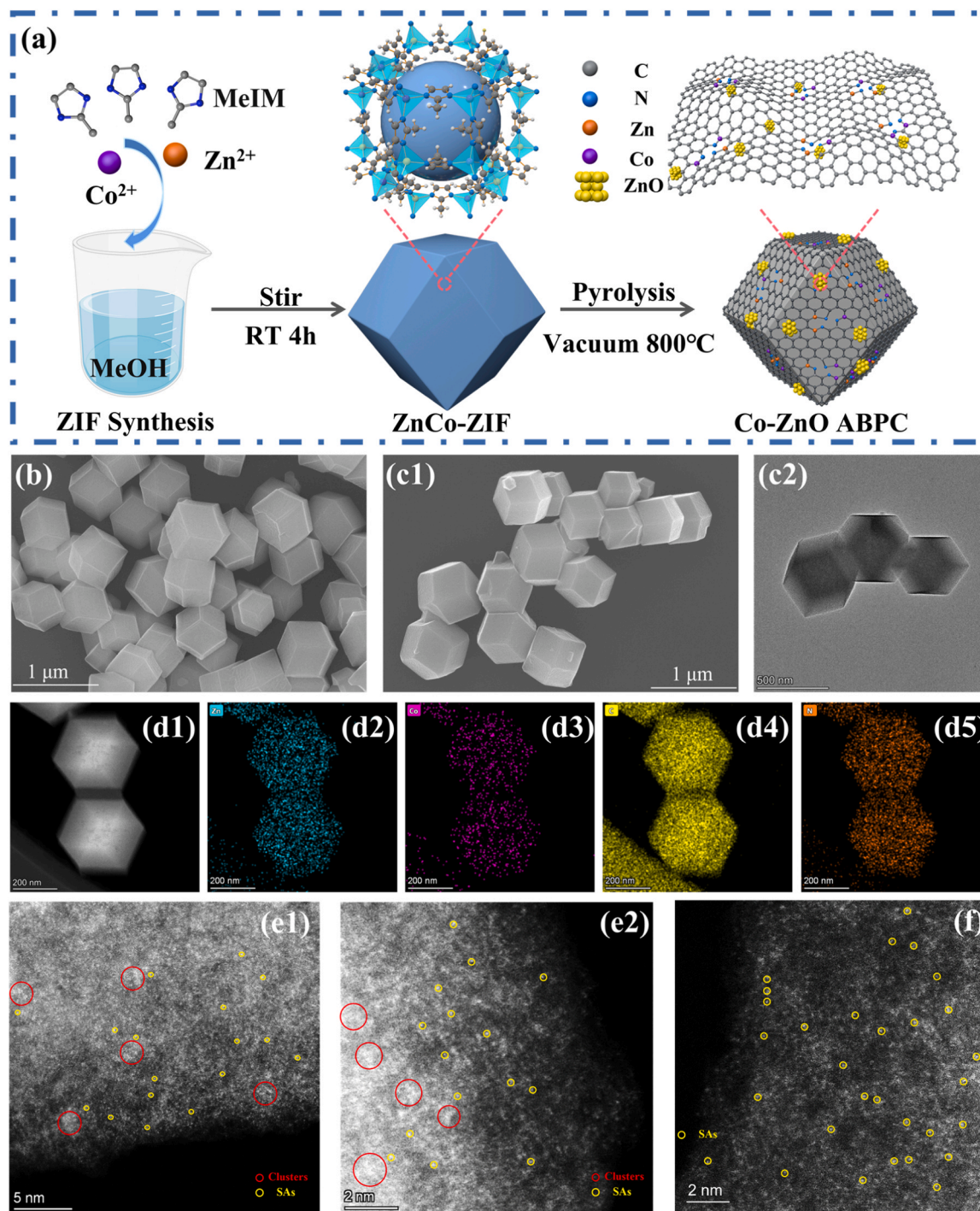

Fig. 1. (a) Schematic illustration of the Co-ZnO ABPC synthesis; (b) SEM images of ZnCo-ZIF; (c1) SEM and (c2) TEM images of Co-ZnO ABPC; (d) HADDF-STEM image (d1) and corresponding STEM-EDX elemental analysis showing elements distribution of Co-ZnO ABPC: Zn (cyan, d2), Co (purple, d3), C (yellow, d4), and N (orange, d5), respectively; (e and f) Aberration-corrected HADDF-STEM image of Co-ZnO ABPC and Co-ZnO ABPC-H.

conditions at 800 °C. The XRD pattern shows that the ZnCo-ZIF precursor owns a ZIF-8 structure (Fig. S1), the results of N_2 sorption isotherms of ZnCo-ZIF demonstrate a microporous characteristic (Fig. S2 and Table S2). SEM of ZnCo-ZIF precursor exhibits a definite rhomboidal dodecahedral shape with smooth surfaces and uniform size distribution (Fig. 1b). The morphology of Co-ZnO ABPC is almost the same prismatic dodecahedral shape as its counterpart precursor (Fig. 1c1), and the TEM result shows no obvious inorganic particles can be detected in Co-ZnO ABPC (Fig. 1c2). The scanning TEM energy dispersive X-ray (STEM-EDX) elemental analysis further confirm that the observed Zn and Co are highly dispersed (Fig. 1d). Moreover, the results of ICP-MS also confirm the presence of Zn and Co in the Co-ZnO ABPC, and the content of Zn and Co are 10.8 wt% and 1.9 wt%, respectively (Table S3). The XRD pattern of Co-ZnO ABPC illustrates that only two peaks at 25° and 44°, corresponding to the (002) and (101) crystal plane diffraction of amorphous carbon, are detected, and there are no any characteristic diffraction peaks of Zn, Co, and ZnO (Fig. S3), which is consistent with the results of the TEM and STEM-EDX [33].

The aberration-corrected HAADF-STEM images (Fig. 1e) of Co-ZnO ABPC reveal the existence of nanoclusters (red circle) and adjacent Zn and Co SAs (yellow circle) on the surface of CN. According to the results of ICP-MS, the content of Zn in Co-ZnO ABPC is significantly higher than that of Co, thus, we tentatively infer that the nanoclusters may be ZnO. To verify this hypothesis, acid etching experiment was conducted because commonly the nanoclusters could be removed whereas the SAs could not [34]. The HAADF-STEM image of the Co-ZnO ABPC after etching by 3 M HCl (denoted as Co-ZnO ABPC-H) shows the disappearance of the nanoclusters (Fig. 1f), while Zn and Co SAs can still be observed. The Zn content of Co-ZnO ABPC-H decreases dramatically to 0.8 wt%, whereas the reduction of the Co amount (from 1.9 wt% to 1.3 wt%) is notably lower than that of Zn. Combining the observations obtained from HAADF-STEM and ICP-MS, one can see that the nanocluster should be ZnO. XPS was employed to analyze the electronic structure of Zn and Co to further confirm the types of nanoclusters and SAs, and the elements Zn, Co, C and N are all identified in Co-ZnO ABPC

(Fig. S4). The high-resolution Zn 2p spectrum of Co-ZnO ABPC and Co-ZnO ABPC-H show similar doublet peaks with a center at ~1021.9 eV (Zn $2p_{3/2}$) and 1044.9 eV (Zn $2p_{1/2}$), corresponding to the Zn^{2+} (Fig. 2a) [35]. However, the peak observed at 988.9 eV in the Zn LMM Auger spectrum of Co-ZnO ABPC, ascribable to ZnO, disappears distinctly after the etching (Fig. 2b) [36,37]. The high-resolution Co 2p spectrum (Fig. 2c) of Co-ZnO ABPC has been deconvoluted into three peaks, which correspond to Co-O (780.4 eV), Co-N (783 eV), and a satellite peak of Co-O (786.2 eV), implying the absence of metallic Co [38]. Furthermore, there are almost no changes in the Co 2p XPS spectrum after the Co-ZnO ABPC was etched. In addition, the N 1 s spectrum of Co-ZnO ABPC can be fitted into five peaks with centers at 398.3, 399.3, 400.5, 401.1, and 402.7 eV originating from pyridinic, metal–N (Co-N and Zn-N), pyrrolic, graphitic, and oxidized nitrogen, respectively (Fig. 2d), which confirms the existence of Co and Zn SAs [39]. Taken together, all these results verify the presence of ZnO nanoclusters on Co-ZnO ABPC, as well as single atoms of Co or Zn SAs, and more importantly, ZnO nanoclusters are positioned in close proximity to SAs. Furthermore, the pure Zn catalyst was also prepared (denoted as Zn-ZnO ABPC) for reference, and the characterizations of Zn-ZnO ABPC show similar morphologies (Fig. S5 and S6) and XPS (Fig. S7) features with Co-ZnO ABPC, indicating the presence of Zn SAs accompanied by adjacent ZnO nanoclusters. After the treatment of acid (denoted as Zn-ZnO ABPC-H), there is only Zn SAs that exist on the surface of Zn-ZnO ABPC-H.

Commonly, metal SAs are regarded as acidic sites whereas ZnO nanoclusters can be basic sites. Therefore, we infer that there are plentiful acidic and basic sites on the surface of Co-ZnO ABPC. To verify this hypothesis, NH_3- and CO_2-TPD were performed. The CO_2-TPD spectra of Co-ZnO ABPC and Zn-ZnO ABPC exhibit two desorption peaks at approximately ~100 °C and 245 °C (Fig. 2e), the low-temperature desorption peak can be attributed to the weaker basic site caused by the N atoms connected with metal SAs, and the desorption of CO_2 at 245 °C should be ascribed to the middle basic sites prompted by the O atoms on the surface of ZnO nanoclusters [40]. After etching, both the
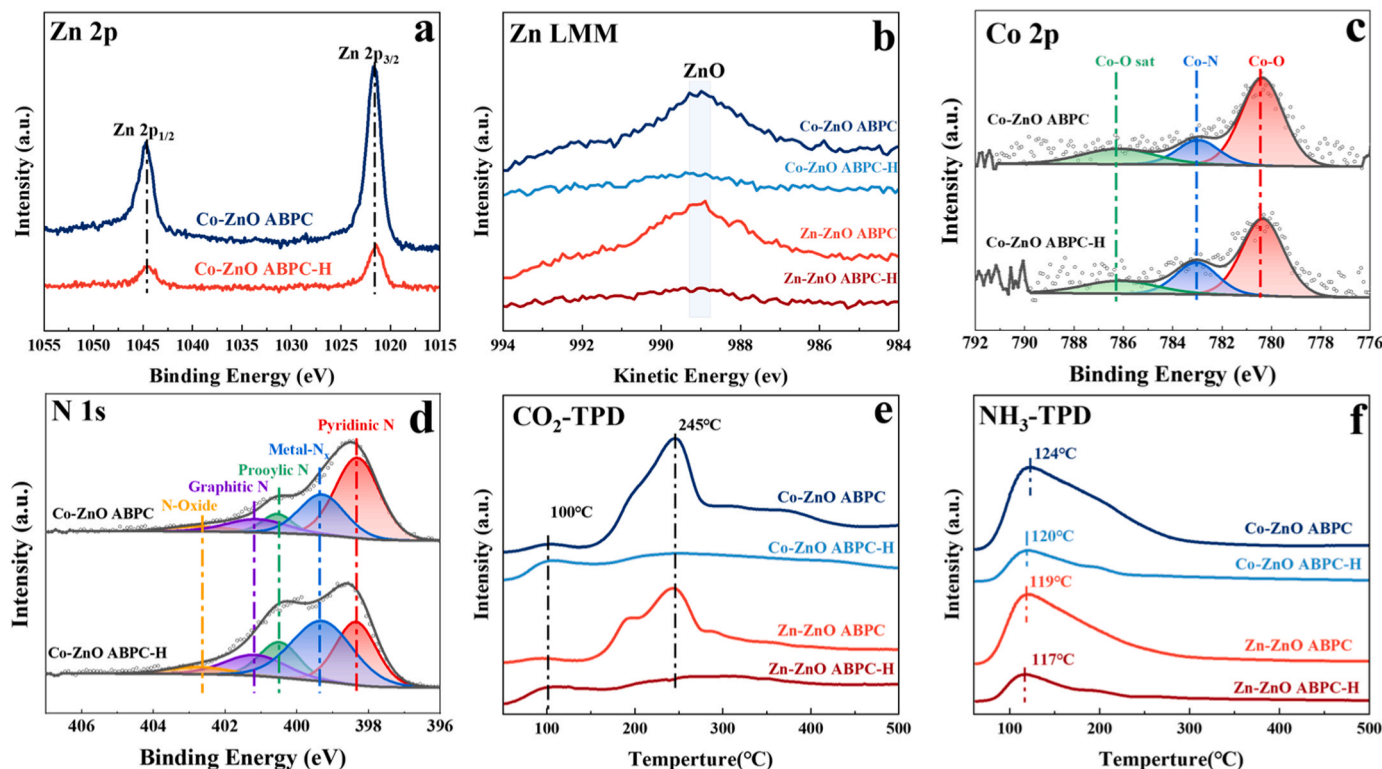

Fig. 2. (a) Zn 2p spectrum; (b) Zn LMM Auger spectrum; (c) Co 2p spectrum; (d) N 1 s spectrum; (e) CO_2-TPD spectra and (f) NH_3-TPD spectra of the obtained NCs.

middle basic sites of Co-ZnO ABPC-H and Zn-ZnO ABPC-H disappeared due to the removal of ZnO nanoclusters, while the weaker basic sites at around ~100 °C remained, which further confirms that the low and middle basic sites are caused by the N atoms and ZnO nanoclusters, respectively. NH$_3$-TPD spectra of Co-ZnO ABPC, Zn-ZnO ABPC, Co-ZnO ABPC-H, and Zn-ZnO ABPC-H show a single peak around ~120 °C that corresponds to NH$_3$ desorption from positive metal ions (Fig. 2f). The significant decrease after etching indicates that NH$_3$ can also be adsorbed onto Zn^{2+} ions on ZnO clusters. Of note, the higher desorption temperatures for Co-ZnO ABPC and Co-ZnO ABPC-H compared to Zn-ZnO ABPC and Zn-ZnO ABPC-H, respectively, suggest that Co ions have stronger acidity than Zn ions. Based on the above analysis, acidic and basic sites are simultaneously introduced to the surface of the CN carrier, and a neighboring Co-ZnO or Zn-ZnO acid-base pairs catalyst is successfully synthesized.

3.2. Catalytic performance toward CHT cascade reaction

Based on the unique neighborhood Co-ZnO acid-base pair structure of Co-ZnO ABPC, we infer that it is well-suited for catalyzing dehydrogenation reactions, including the oxidation of alcohols and other related reactions. Combined with our previous work [5], the CHT cascade reaction for imine synthesis by benzyl alcohol and nitrobenzene was chosen as a model reaction to explore the catalytic performance of the Co-ZnO ABPC. The CHT cascade reaction was evaluated at 160 ℃ for 3 h under a N$_2$ atmosphere with a nitrobenzene to benzyl alcohol molar ratio of 1/3. The conversion of nitrobenzene and the selectivity of imine reached 95 % and 98 %, respectively (Table 1, entry 1). Furthermore, the nitrobenzene conversion and imine selectivity values of 61 % and 98 % were achieved (Table 1, entry 7), respectively, at 120 ℃ for 12 h, dramatically outperforming currently reported advanced non-noble-metal catalysts and even compared to the noble-metal catalysts. The ZnCo-N$_2$/CN catalyst, prepared by calcination of the ZnCo-ZIF precursor under N$_2$, exhibited inferior activity and turnover frequencies (TOF) value compared to Co-ZnO ABPC at both 120 °C and 160 °C (Table S4 and S5). This can be attributed to the formation of a carbon layer on the catalyst surface during the calcination process (Table S3 and Fig S8), hindering the exposure of active sites, which undoubtedly proves the superiority of the preparation method under vacuum conditions.

Parallel experiments were employed to gain further insight into the function of the acid-base pair. As a reference, catalysts of solely Co SAs or ZnO loaded on carbon carriers (Co SAC/CN and ZnO/AC) were prepared. To explore the clear difference among the catalysts, the CHT cascade reactions were all carried out at 120 °C for 12 h. In stark contrast to Co-ZnO ABPC, Co-ZnO ABPC-H (Co and Zn SAs), Zn-ZnO ABPC-H (Zn SAs), Co SAC/CN (Co SAs), and ZnO/AC (ZnO nanoparticles) all exhibited no catalytic activity (Table 1, entries 2–5), indicating that the catalysts with only acidic or basic sites have no catalysis capacities for the CHT cascade reaction. To verify this deduction, external base K$_2$CO$_3$ was added, which alone did not exhibit any catalytic activity for this reaction (Table 1, entry 12). Of note, all the acidic sites catalysts, Co-ZnO ABPC-H, Zn-ZnO ABPC-H, and Co SAC/CN, exhibited enhanced catalytic activities, and the conversion of nitrobenzene are 76 %, 14 %, and 75 % (Table 1, entries 9–11), respectively, which undoubtedly confirms that the acid-base pair is essential for the occurrence of the CHT cascade reaction. Furthermore, the catalytic activity of Co-ZnO ABPC also can be significantly increased when K$_2$CO$_3$ is added, and the conversion of nitrobenzene is enhanced from 61 % to 98 % (Table 1, entry 8). Besides, the trend of the strength of the exogenous bases (Cs$_2$CO$_3$ > K$_2$CO$_3$ > Na$_2$CO$_3$) is almost identical to the catalytic activity (Fig. S9), which further highlights the importance of basic sites in the CHT cascade reaction. All the above results confirm that the ZnO clusters on the surface of Co-ZnO ABPC serve as a "fixed" alkaline site near the acidic metal sites, and that it is the synergistic effect of metallic SAs and ZnO nanoclusters that promotes the outstanding catalytic performance of Co-ZnO ABPC.

Similarly, Zn-ZnO ABPC (Zn SAs with ZnO nanoclusters) achieved nitrobenzene conversion of 17 % and imine selectivity of 100 % (Table 1, entries 6), and the TOF value of 3.49 h^{-1} obviously smaller than that of Co-ZnO ABPC (8.01 h^{-1}), demonstrating the combination of Zn SAs and ZnO clusters also can catalyze the CHT cascade reaction. While the lower catalytic activity of Zn-ZnO ABPC than that of Co-ZnO ABPC illustrates the inferior catalytic capacity of Zn SAs compared to Co SAs, in coincidence with the observations in K$_2$CO$_3$ control experiments, which might be caused by the relatively weak acidity of Zn SAs. Taken together, Zn-ZnO or Co-ZnO acid-base pairs on the surface of Co-ZnO ABPC are the active site for the catalysis of the CHT cascade reaction, and Co-ZnO acid-base pair plays a more significant role.

To check the reusability and stability of the Co-ZnO ABPC, we performed a recycling test (Fig. S10). After three cycles, the conversion of nitrobenzene and selectivity of imine decreased from 95 % and 98–47 % and 96 %, respectively. However, TEM images (Fig. S11) showed that the recovered Co-ZnO ABPC still maintains a definite rhomboidal dodecahedral shape and micro-morphologies after three cycles. Therefore, we infer that the decrease in catalytic activity may be primarily caused by the coverage of the active site due to the adsorption of organic reactants and products [41]. For verifying this hypothesis, the recovered catalyst was recalcined at 800 °C for 3 h under vacuum to remove the adsorbed organic reactants and products, and its catalytic performance was re-assessed. The regenerated Co-ZnO ABPC catalyst regains the outstanding catalytic performance, and 89 % nitrobenzene conversion and 98 % imine selectivity are reached (Fig. S10). In addition, the analyses of ICP-MS, TEM, and aberration-corrected HADDF-STEM for the regenerated catalyst were also performed to further confirm the structural stability of Co-ZnO ABPC, and the results show that the recalcined Co-ZnO ABPC remains almost the same Co SAs and ZnO nanoclusters structures and the contents of Co and Zn (Fig. S12 and S13). Taken together, one can see that the Co-ZnO ABPC catalyst possesses excellent stability.

Inspired by the remarkable performance of Co-ZnO ABPC, we extended our attention to different types of aromatic alcohols and substituted nitrobenzene derivatives to explore the substrate scope of the CHT cascade reactions catalyzed by Co-ZnO ABPC. As listed in Table 2, the hydrogen atoms of both aromatic and heteroaromatic alcohols with different substituents can be transferred to nitrobenzene to smoothly obtain the corresponding imines (Table 2, entries 2–8 f). Of note, the lower activity for heteroaromatic alcohols may be due to the higher electronic density of heterocyclic compounds, which leads to a more difficult removal of H in the alcohol. In addition, nitrobenzene derivatives are well tolerated under the reaction conditions (Table 2, entries 9–16 f), with those containing electron-donating groups showing relatively higher yields than those containing electron-withdrawing groups. These results suggest that Co-ZnO ABPC possesses exceptional stability and universality.

3.3. First principle calculations

First principle calculations based on density functional theory were performed to theoretically understand the synergistic effect of the SAs and ZnO clusters in the Co-ZnO ABPC for catalyzing the CHT cascade reactions. Note that the dehydrogenation process is the rate-determining step in the CHT cascade reactions according to our previous works. Thus, the process of the first dehydrogenation of benzyl alcohol on the catalysts was focused in this study. The dehydrogenation reaction can be classified into two steps. The first step corresponds to the dehydrogenation of hydroxyl of benzyl alcohol, and the activated hydroxyl H atom will shift to the adjacent base site of the catalysts itself. However, only the activated H atom on the catalyst can be utilized by nitrobenzene to promote its reduction, which corresponds to the dehydrogenation of the catalyst and is considered the second step.

As shown in Fig. 3a, the adsorption energy of benzyl alcohol on the

Table 2
Products and conversions of imines synthesis by CHT cascade reaction catalyzed by Co-ZnO ABPC.

1f, 3h, 95%[a] (98%[b])　　2f, 3h, 87% (95%)　　3f, 3h, 90% (95%)　　4f, 3h, 89% (97%)

5f, 6h, 91% (97%)　　6f, 3h, 76% (>99%)　　7f, 6h, 85% (99%)　　8f, 12h, 73% (95%)

9f, 3h, 95% (97%)　　10f, 6h, 91% (>99%)　　11f, 3h, 88% (97%)　　12f, 3h, 97% (96%)

13f, 3h, 85% (99%)　　14f, 6h, 83% (93%)　　15f, 3h, 93% (97%)　　16f, 12h, 85% (93%)

Reaction conditions: 3 mmol alcohols, 1 mmol nitro compounds, Co-ZnO ABPC (20 mg), toluene (1 ml), 160 °C, N2. [a] Nitro-compounds conversions were determined by GC and [b] selectivities towards the aimed imines based on the yields and nitro-compounds conversions.
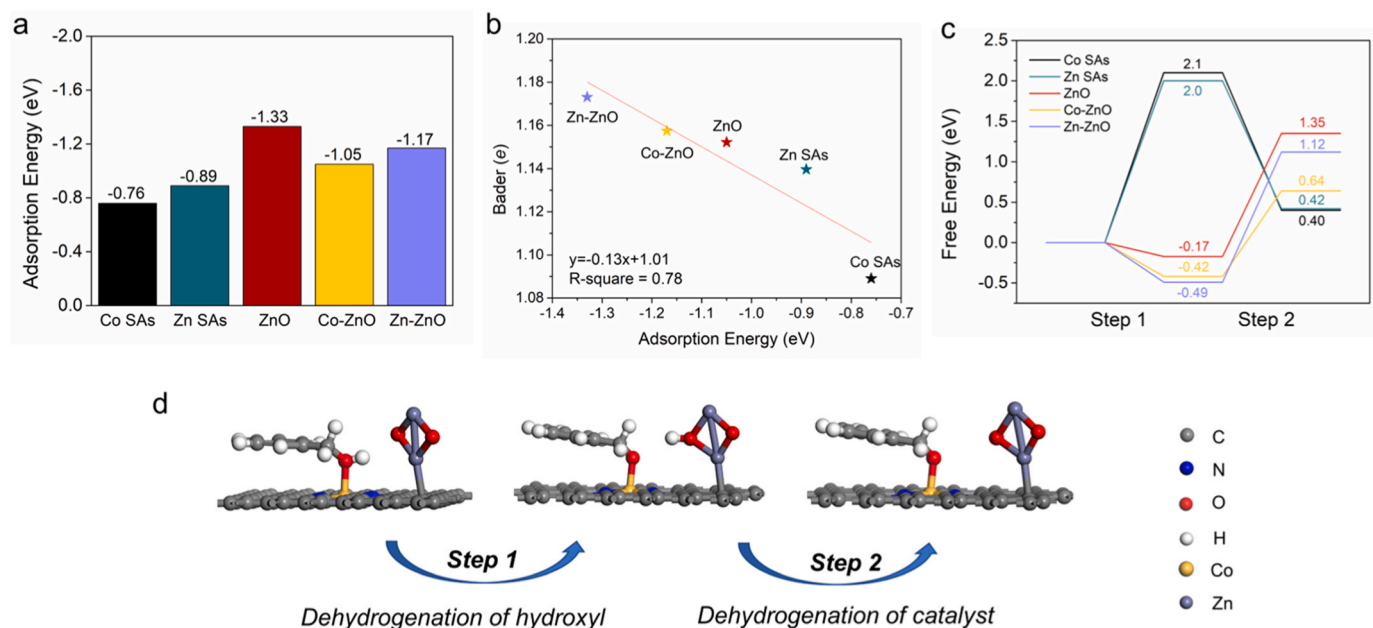

Fig. 3. (a) Adsorption energy of benzyl alcohol on the surfaces of catalysts. (b) The relationship of the electron accumulation of the O atom in the hydroxyl group of benzyl alcohol and its adsorption energy on the surfaces of catalysts. (c-d) Free energy pathway and illustration of dehydrogenation of hydroxyl and dehydrogenation of catalysts on the different surfaces of catalysts.

surfaces of Co SAs, Zn SAs, ZnO, Co-ZnO ABPC, and Zn-ZnO ABPC substrates was firstly calculated. The results show that the acidic site of Co or Zn SAs is the adsorption site for the benzyl alcohol by the interaction with the electrons-rich oxygen atom in the hydroxyl group of benzyl alcohol. Of note, the adsorption energies of benzyl alcohol on the surfaces of both SAs increase with the participation of the ZnO clusters. Through the Bader charge analysis, we found that the electron accumulation of the oxygen atom in the hydroxyl group of adsorbed benzyl

alcohol is positively proportional to the adsorption energy of benzyl alcohol on the five catalysts (Fig. 3b). The more electrons accumulate in the oxygen atom of the hydroxyl group in the catalysts adsorption systems, the bigger the adsorption energies it is. Generally speaking, the increased adsorption energies of benzyl alcohol on the catalysts indicate the intense interactions between them, which can significantly weaken the bonding strength of the benzyl alcohol, and thus facilitating the dehydrogenation reaction. Then, the free energy pathway of the dehydrogenation reaction of benzyl alcohol on these substrates is established to further explore the catalytic performance of the five catalysts.

As shown in Fig. 3c-d and Fig. S14, for the SAs-type catalysts (Zn-ZnO ABPC-H and Co SAC/CN), the limiting step is the dehydrogenation of hydroxyl of benzyl alcohol due to its very high energy barrier (~2 eV) caused by insufficient alkaline sites. However, the activated H atom desorption on the SAs-type catalyst is easy, possibly due to the weak interaction between the H atom and the coordination N atom. In contrast, the ZnO catalyst can powerfully activate the hydroxyl H atom of the benzyl alcohol, but it encounters a high energy barrier (1.52 eV) in the second step. Interestingly, the Co-ZnO ABPC and Zn-ZnO ABPC possess a smaller energy barrier for the complete two steps than that of the pure SAs or ZnO catalysts. Due to the stronger acidity of Co SAs and its synergistic effect with ZnO clusters, Co-ZnO ABPC embraces the smallest free energy barrier (1.06 eV) for the dehydrogenation reaction of benzyl alcohol on these five substrates, thereby exhibiting the best performance in the CHT cascade reactions. Based on the theoretical calculations, we can conclude that the absence of basic sites will make the hydrogen activation on hydroxyl become a rate-limiting step, while the too-strong binding energy will make it difficult for H to be utilized by nitrobenzene. The catalysts, such as Co-ZnO ABPC with both acid-base sites and moderate adsorption energy towards benzyl alcohol can produce the best catalytic performance.

3.4. Insight into the catalytic mechanism

Based on the results of the experiments and theoretical calculations, the proposed CHT cascade reaction mechanism over Co-ZnO ABPC is illustrated in Scheme 2. Co-ZnO acid-base pair (active site A, Scheme 2) is identified as the main active site for the CHT cascade reaction. Initially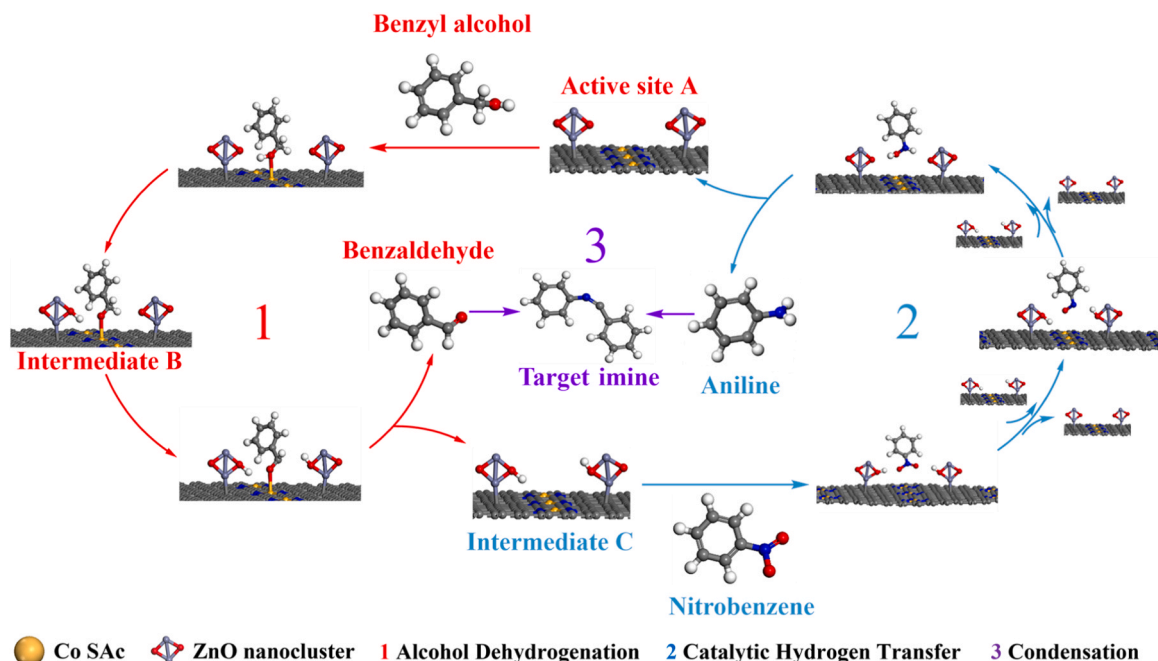, the nucleophilic hydroxyl O atom of benzyl alcohol is preferentially connected with the Co SAs acidic site (step 1, Scheme 2), followed by the O-H bond activation. After that, the H atom on the hydroxyl group transfers to the adjacent O atom of the basic site ZnO (intermediate B), and the α-H on the methylene group of the hydroxymethyl is also removed to form intermediate C and produces benzaldehyde. Subsequently, nitrobenzene is gradually reduced to form PhNO (niteosobenzene), PhNHOH (phenylhydroxylamine), and final PhNH₂ (aniline) in turn (step 2, Scheme 2) [42–44], meanwhile, intermediate B releases protons and reverts back to active site A for the next oxidation circulation of benzyl alcohol. Once aniline forms, it immediately reacts with benzaldehyde to yield the target imine (step 3, Scheme 1).

4. Conclusions

In this study, a novel Co-ZnO acid-base pair catalyst, containing numerous adjacent Co-ZnO or Zn-ZnO acid-base pairs on the surface, was prepared by controlled calcining a bimetallic ZnCo-ZIF precursor with an appropriate Zn/Co ratio under vacuum. Co-ZnO ABPC exhibited exceptional catalytic performance for the CHT cascade reaction between nitrobenzene and benzyl alcohol at 160 °C, the conversion efficiency of nitrobenzene and the selectivity of imine could reach up to 95 % and 98 %, respectively, in 3 h. Furthermore, the Co-ZnO ABPC also displayed remarkable catalytic activity at low temperatures, making it the most advanced non-noble-metal catalyst for CHT cascade reaction. Additionally, Co-ZnO ABPC demonstrated remarkable durability and universality. First principle calculations confirm that the superior catalytic activity of Co-ZnO ABPC mainly takes advantage of its unique adjacent Co-ZnO acid-base pair structure, resulting in minimal free energy barriers. This work is highly instructive for the design and synthesis of efficient acid-base pair catalysts and provides significant insight into the effects of the characteristics of acid-base pair on CHT cascade reaction.

CRediT authorship contribution statement

Tianshuai Wang and **Hepeng Zhang**: conceived the idea. **Hepeng Zhang**, **Tianshuai Wang** and **Qiuyu Zhang** supervised the project. **Zhanwei Chen** and **Chen Wu** prepared the catalysts and performed the catalytic tests. **Tianshuai Wang** contributed to the DFT calculations and data analysis. **Zhanwei Chen**, **Chen Wu**, **Wenrui Li**, **Shaowei Yang** and

Scheme 2. Proposed CHT cascade reaction mechanism over Co-ZnO ABPC.

Haidong Shen performed the catalyst characterizations. **Zhanwei Chen** and **Runze Gao** organized data. **Zhanwei Chen**, **Tianshuai Wang** and **Hepeng Zhang** wrote the paper with input from all authors. All authors discussed the results and commented on the manuscript.

Declaration of Competing Interest

The authors declare no competing financial interest.

Data availability

Data will be made available on request.

Acknowledgments

Appendix A. Supporting information

Supplementary data associated with this article can be found in the online version at doi:10.1016/j.apcatb.2023.123203.

References

[1] R.H. Beddoe, K.G. Andrews, V. Magné, J.D. Cuthbertson, J. Saska, A.L. Shannon-Little, S.E. Shanahan, H.F. Sneddon, R.M. Denton, Redox-neutral organocatalytic Mitsunobu reactions, Science 365 (2019) 910–914.
[2] G.-Jt Brink, I.W.C.E. Arends, R.A. Sheldon, Green, catalytic oxidation of alcohols in water, Science 287 (2000) 1636–1639.
[3] X.-R. Tian, X.-L. Jiang, S.-L. Hou, Z.-H. Jiao, J. Han, B. Zhao, Selectively regulating Lewis acid–base sites in metal–organic frameworks for achieving turn-on/off of the catalytic activity in different CO$_2$ reactions, Angew. Chem. Int. Ed. 61 (2022) e202200123.
[4] H. Chen, S. He, M. Xu, M. Wei, D.G. Evans, X. Duan, Promoted synergic catalysis between metal Ni and acid–base sites toward oxidant-free dehydrogenation of alcohols, ACS Catal. 7 (2017) 2735–2743.
[5] C. Wu, C. Zhu, K. Liu, S. Yang, Y. Sun, K. Zhu, Y. Cao, S. Zhang, S. Zhuo, M. Zhang, Q. Zhang, H. Zhang, Nano-pyramid-type Co-ZnO/NC for hydrogen transfer cascade reaction between alcohols and nitrobenzene, Appl. Catal. B Environ. 300 (2022), 120288.
[6] H. Zhou, H. Xu, Y. Liu, Aerobic oxidation of 5–hydroxymethylfurfural to 2,5-furandicarboxylic acid over Co/Mn-lignin coordination complexes-derived catalysts, Appl. Catal. B Environ. 244 (2019) 965–973.
[7] F. Neațu, R.S. Marin, M. Florea, N. Petrea, O.D. Pavel, V.I. Pârvulescu, Selective oxidation of 5-hydroxymethyl furfural over non-precious metal heterogeneous catalysts, Appl. Catal. B Environ. 180 (2016) 751–757.
[8] B. Chen, L. Wang, S. Gao, Recent advances in aerobic oxidation of alcohols and amines to imines, ACS Catal. 5 (2015) 5851–5876.
[9] Y. Wang, T. Wei, Y. Qu, Y. Zhou, Y. Zheng, C. Huang, Y. Zhang, Q. Yu, H. Chen, Smart, photothermally activated, antibacterial surfaces with thermally triggered bacteria-releasing properties, ACS Appl. Mater. Interfaces 12 (2020) 21283–21291.
[10] Y. Bu, L. Zhang, J. Liu, L. Zhang, T. Li, H. Shen, X. Wang, F. Yang, P. Tang, D. Wu, Synthesis and properties of hemostatic and bacteria-responsive in situ hydrogels for emergency treatment in critical situations, ACS Appl. Mater. Interfaces 8 (2016) 12674–12683.
[11] W. Xie, S. Huang, D. Tang, S. Liu, J. Zhao, Biomass-derived Schiff base compound enabled fire-safe epoxy thermoset with excellent mechanical properties and high glass transition temperature, Chem. Eng. J. 394 (2020), 123667.
[12] S. Xie, T. Xia, S. Li, C. Mo, M. Chen, X. Li, Bacteria-propelled microrockets to promote the tumor accumulation and intracellular drug uptake, Chem. Eng. J. 392 (2020) 123786.
[13] K. Zhu, Z. Li, F. Cheng, C. Wu, D. Cai, Q. Zhang, H. Zhang, Preparation of durable superhydrophobic composite coatings with photothermal conversion precisely targeted configuration self-healability and great degradability, Compos. Sci. Technol. 213 (2021), 108926.
[14] G. Liu, D.A. Cogan, T.D. Owens, T.P. Tang, J.A. Ellman, Synthesis of enantiomerically pure N-tert-butanesulfinyl imines (tert-butanesulfinimines) by the direct condensation of tert-butanesulfinamide with aldehydes and ketones, J. Org. Chem. 64 (1999) 1278–1284.
[15] H. Li, A. Al-Dakhil, D. Lupp, S.S. Gholap, Z. Lai, L.-C. Liang, K.-W. Huang, Cobalt-catalyzed selective hydrogenation of nitriles to secondary imines, Org. Lett. 20 (2018) 6430–6435.
[16] G. Liang, Y. Zhou, J. Zhao, A.Y. Khodakov, V.V. Ordomsky, Structure-sensitive and insensitive reactions in alcohol amination over nonsupported Ru nanoparticles, ACS Catal. 8 (2018) 11226–11234.
[17] Z. Li, X. Lu, R. Zhao, S. Ji, M. Zhang, J.H. Horton, Y. Wang, Q. Xu, J. Zhu, A. Heterogeneous, Single atom cobalt catalyst for highly efficient acceptorless dehydrogenative coupling reactions, Small 19 (2023) 2207941.
[18] S. Yang, H. Shen, F. Cheng, C. Wu, Y. Cao, S. Zhuo, Q. Zhang, H. Zhang, Organometallic precursor induced defect-enriched mesoporous CeO$_2$ with high specific surface area: preparation and catalytic performance, J. Mater. Chem. A 8 (2020) 14006–14014.
[19] H. Zhang, C. Wu, W. Wang, J. Bu, F. Zhou, B. Zhang, Q. Zhang, Effect of Ceria on redox-catalytic property in mild condition: a solvent-free route for imine synthesis at low temperature, Appl. Catal. B Environ. 227 (2018) 209–217.
[20] D. Liu, P. Yang, H. Zhang, M. Liu, W. Zhang, D. Xu, J. Gao, Direct reductive coupling of nitroarenes and alcohols catalysed by Co–N–C/CNT@AC, Green. Chem. 21 (2019) 2129–2137.
[21] J. Chen, S. Huang, J. Lin, W. Su, Recyclable palladium catalyst for facile synthesis of imines from benzyl alcohols and nitroarenes, Appl. Catal. A Gen. 470 (2014) 1–7.
[22] D.-W. Tan, H.-X. Li, D.J. Young, J.-P. Lang, Phosphine ligand-free RuCl$_3$-catalyzed reductive N-alkylation of aryl nitro compounds, Tetrahedron 72 (2016) 4169–4176.
[23] M. Sankar, Q. He, S. Dawson, E. Nowicka, L. Lu, P.C.A. Bruijnincx, A.M. Beale, C.J. Kiely, B.M. Weckhuysen, Supported bimetallic nano-alloys as highly active catalysts for the one-pot tandem synthesis of imines and secondary amines from nitrobenzene and alcohols, Catal. Sci. Technol. 6 (2016) 5473–5482.
[24] T. Song, J.E. Park, Y.K. Chung, Rhodium-catalyzed synthesis of imines and esters from benzyl alcohols and nitroarenes: change in catalyst reactivity depending on the presence or absence of the phosphine ligand, J. Org. Chem. 83 (2018) 4197–4203.
[25] K.-i Shimizu, K. Kon, M. Seto, K. Shimura, H. Yamazaki, J.N. Kondo, Heterogeneous cobalt catalysts for the acceptorless dehydrogenation of alcohols, Green. Chem. 15 (2013) 418–424.
[26] S.M.A. Hakim Siddiki, T. Toyao, K.-i Shimizu, Acceptorless dehydrogenative coupling reactions with alcohols over heterogeneous catalysts, Green. Chem. 20 (2018) 2933–2952.
[27] W.H. Cheng, S. Akhter, H.H. Kung, Structure sensitivity in methanol decomposition on ZnO single-crystal surfaces, J. Catal. 82 (1983) 341–350.
[28] Y. Shinohara, T. Nakajima, S. Suzuki, A theoretical study of the dehydration and the dehydrogenation processes of alcohols on metal oxides using MOPAC, J. Mol. Struct.: Theochem. 460 (1999) 231–244.
[29] M.V. Morales, E. Asedegbega-Nieto, A. Iglesias-Juez, I. Rodríguez-Ramos, A. Guerrero-Ruiz, Role of exposed surfaces on zinc oxide nanostructures in the catalytic ethanol transformation, ChemSusChem 8 (2015) 2223–2230.
[30] J. Hafner, Ab-initio simulations of materials using VASP: density-functional theory and beyond, J. Comput. Chem. 29 (2008) 2044–2078.
[31] J. Moellmann, S. Grimme, DFT-D3 study of some molecular crystals, J. Phys. Chem. C. 118 (2014) 7615–7621.
[32] P. Wisesa, K.A. McGill, T. Mueller, Efficient generation of generalized Monkhorst-Pack grids through the use of informatics, Phys. Rev. B 93 (2016), 155109.
[33] C. Ma, J. Wang, F. Wang, Y. Zhu, Y. Li, X. Fan, F. Zhang, G. Zhang, W. Peng, Facile synthesis of iron oxide supported on porous nitrogen doped carbon for catalytic oxidation, Sci. Total Environ. 785 (2021), 147296.
[34] Z. Ma, S. Liu, N. Tang, T. Song, K. Motokura, Z. Shen, Y. Yang, Coexistence of Fe nanoclusters boosting Fe single atoms to generate singlet oxygen for efficient aerobic oxidation of primary amines to imines, ACS Catal. 12 (2022) 5595–5604.
[35] Z. Lu, B. Wang, Y. Hu, W. Liu, Y. Zhao, R. Yang, Z. Li, J. Luo, B. Chi, Z. Jiang, M. Li, S. Mu, S. Liao, J. Zhang, X. Sun, An isolated zinc–cobalt atomic pair for highly active and durable oxygen reduction, Angew. Chem. Int. Ed. 58 (2019) 2622–2626.
[36] M. Li, G. Meng, Q. Huang, S. Zhang, Improved sensitivity of polychlorinated-biphenyl-orientated porous-ZnO surface photovoltage sensors from chemisorption-formed ZnO-CuPc composites, Sci. Rep. 4 (2014) 4284.
[37] M. Norman, P. Bartczak, J. Zdarta, W. Tylus, T. Szatkowski, A.L. Stelling, H. Ehrlich, T. Jesionowski, Adsorption of C.I. natural red 4 onto spongin skeleton of marine demosponge, Mat 8 (2015) 96–116.
[38] S. Yang, C. Wu, J. Wang, H. Shen, K. Zhu, X. Zhang, Y. Cao, Q. Zhang, H. Zhang, Metal single-atom and nanoparticle double-active-site relay catalysts: design, preparation, and application to the oxidation of 5-hydroxymethylfurfural, ACS Catal. 12 (2022) 971–981.
[39] Y.-N. Li, Z. Sun, T. Zhang, ACS Appl. Mater. Interfaces 15 (2023) 1432–1441.
[40] B. Wang, M. Li, S. Zhang, H. Wu, Y. Liao, H. Li, Synergistic effect between Co single atoms and nanoparticles enables selective synthesis of bio-based benzimidazoles, Appl. Catal. B Environ. 327 (2023), 122454.
[41] M.D. Argyle, C.H. Bartholomew, Heterogeneous catalyst deactivation and regeneration: a review, Catalysts 5 (2015) 145–269.
[42] W. Xiong, Z. Wang, S. He, F. Hao, Y. Yang, Y. Lv, W. Zhang, P. Liu, Ha Luo, Nitrogen-doped carbon nanotubes as a highly active metal-free catalyst for nitrobenzene hydrogenation, Appl. Catal. B Environ. 260 (2020), 118105.
[43] S. Tian, M. Hu, Q. Xu, W. Gong, W. Chen, J. Yang, Y. Zhu, C. Chen, J. He, Q. Liu, H. Zhao, D. Wang, Y. Li, Single-atom Fe with Fe$_1$N$_3$ structure showing superior performances for both hydrogenation and transfer hydrogenation of nitrobenzene, Sci. China Mater. 64 (2021) 642–650.
[44] C. Wang, B. Ye, R. Zhou, Y. Jiang, Z. Hou, Structure–activity relationship for the catalytic hydrogenation of nitrobenzene by single platinum atoms supported on nitrogen-doped carbon, ACS Appl. Nano Mater. 5 (2022) 13601–13611.